

Electron-Mass Anisotropy in Type-III HgZnTe-CdTe Superlattices

J. M. Berroir, Y. Guldner, J. P. Vieren, and M. Voos

Département de Physique de l'Ecole Normale Supérieure, 24 rue Lhomond, 75231 Paris, France

X. Chu and J. P. Faurie

Department of Physics, University of Illinois at Chicago, Chicago, Illinois 60680

(Received 2 February 1989)

Cyclotron-resonance experiments done in a novel superlattice, HgZnTe-CdTe, provide the first determination of the conduction-band dispersion in a type-III superlattice. The measured electron-mass anisotropy is strongly dependent on the CdTe layer thickness, in agreement with band-structure and Landau-level calculations. These calculations show also that the studied superlattices are semimetallic, consistent with the large valence-band offset (300 meV). Another cyclotron-resonance transition is observed, evidencing strongly the formation of a two-dimensional electron gas.

PACS numbers: 73.40.Lq, 73.20.Dx, 78.20.Ls

II-VI superlattices (SL) formed with CdTe and a zero-gap mercury-based compound have been termed "type-III" SL's because of the unique inverted band structure of the zero-gap material. They can be semiconducting or semimetallic,¹ depending on the layer thickness and on the valence-band offset Λ , as noted previously in HgTe-CdTe SL's. High electron and hole mobilities^{2,3} have been reported in some type-III SL's, corresponding to the extremely small in-plane electron and hole effective masses in the nearly zero-gap SL's. Investigations of the carrier dispersion relations in the plane of the layers and along the SL axis are of particular interest in these novel systems and can be achieved by cyclotron-resonance experiments, as reported in GaAs-AlGaAs⁴ and in *p*-type HgTe-CdTe SL's.⁵ Here we describe the first cyclotron-resonance measurements on high-electron-mobility HgZnTe-CdTe SL's grown by molecular-beam epitaxy (MBE) in the [100] direction. The SL electron cyclotron resonance is observed for magnetic fields both perpendicular and parallel to the growth axis. We show that band-structure and Landau-level calculations, which are absolutely necessary to understand the unusual features of type-III SL's, can account for the data, in particular for the observed mass anisotropy, if the samples are semimetallic. From these results, the value of the valence-band offset in this new system is discussed. A second electron cyclotron-resonance transition is observed, evidencing a charge transfer from the CdTe buffer layer to the SL and the

formation of a two-dimensional electron gas (2DEG).

The SL's were grown by MBE on a (100) GaAs substrate with a 2- μ m CdTe buffer layer⁶ and consist of one hundred periods of Hg_{1-x}Zn_xTe-CdTe. The CdTe layers contain up to 15% HgTe.⁷ For each sample, the layer thicknesses and the alloy Zn composition, as well as the electron mobility μ and concentration at 25 K, are listed in Table I. The samples were prepared intentionally with thin CdTe barriers to study the carrier transport along the SL axis and were *n* type in the temperature range investigated (2–300 K), with Hall mobilities in excess of 2×10^5 cm²/Vs at low temperature.

At first we discuss the SL band structure and Landau levels calculated in the envelope-function approximation, as reported for HgTe-CdTe SL's.⁸ The band parameters for CdTe are given in Ref. 8. For Hg_{1-x}Zn_xTe, the Γ_6 - Γ_8 energy separation is extrapolated using $x \approx 0.12$ for the semimetal-semiconductor transition at 2 K,⁹ while the higher band parameters were taken identical to those of HgTe. Figure 1 presents the band structure of sample *S*₁ in the plane of the layers (k_x) and along the SL growth axis (k_z). The calculations are done for the two controversial values¹ of Λ in HgTe-CdTe SL's (≈ 40 meV^{8,10} and ≈ 300 meV¹¹). E_1 , LH₁ (HH₁, HH₂) denote the first light-particle (heavy-hole) bands along k_z , respectively. The zero of energy is taken at the CdTe valence-band edge. For $\Lambda = 40$ meV [Fig. 1(a)], *S*₁ is a semiconductor, E_1 being the conduction band, and HH₁ the highest valence band. For $\Lambda = 300$

TABLE I. Characteristics of the superlattices used in this work. d_1 and d_2 are the HgZnTe and CdTe layer thicknesses, respectively, and x is the Zn composition; n and μ are measured at 25 K.

| Sample | d_1 (Å) | d_2 (Å) | x | μ (cm ² /Vs) | n (cm ⁻³) |
|-----------------------|--------------|--------------|-------|--------------------------------|----------------------------|
| <i>S</i> ₁ | 105 | 20 | 0.053 | 2.1×10^5 | 3.7×10^{15} |
| <i>S</i> ₂ | 80 | 12 | 0.053 | 2.1×10^5 | 2.6×10^{15} |

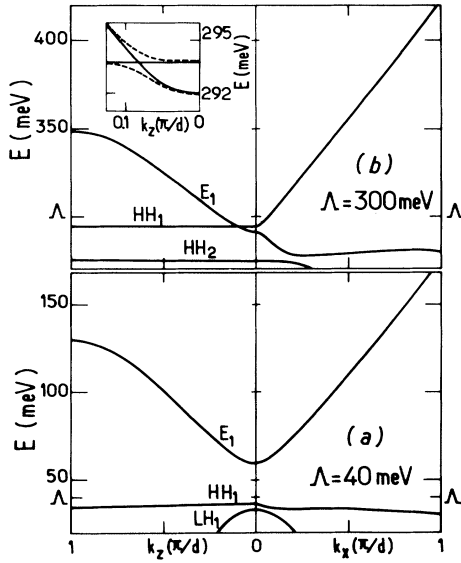


FIG. 1. Calculated band structure of S_1 (solid lines), which is magnified in the inset for small k_z . The dashed line in the inset represents schematically the HH_1 - E_1 anticrossing.

meV [Fig. 1(b)], HH_1 and E_1 exchange roles along k_x and the SL is semimetallic with a small negative energy gap (≈ -2 meV). The most remarkable change between the two calculated band structures is the conduction-band dispersion along k_z . For $\Lambda = 40$ meV, the calculated conduction effective mass m_z along k_z is extremely small and the conduction band is nearly isotropic around $k=0$. On the contrary, for $\Lambda = 300$ meV, it is dispersionless for $0 < k_z < 0.1\pi/d$, corresponding to a strong band anisotropy near $k=0$. There is, in fact, a small anticrossing between HH_1 and E_1 along k_z due to the k -linear terms that we have neglected. Such an anticrossing is also obtained in the LCAO calculations³ reported in HgTe-CdTe SL's. The resulting dispersion of the conduction band is schematically represented in the inset of Fig. 1(b). m_z is much larger than in the former case ($\Lambda = 40$ meV) while the in-plane mass m_x is extremely small near $k_x = 0$ ($\approx 2 \times 10^{-3} m_0$), as a result of the small HH_1 - E_1 separation.¹ From Fig. 1, it is clear that the nature of the SL (semiconductor or semimetallic) can be deduced from the measurement of the electron mass-anisotropy ratio m_z/m_x near $k=0$, for instance from low-magnetic-field cyclotron-resonance measurements. Note that when we include in the calculations the strain effects due to the 0.6% lattice mismatch between the host materials as described in Refs. 12-14, assuming that the SL lattice constant is the same as that of the CdTe buffer layer, S_1 and S_2 are found to be semiconductors even for $\Lambda = 300$ meV. But, in addition, if one takes into account the presence of 15% of HgTe in the CdTe layers,⁷ the resulting band structure is quite identical to that shown in Fig. 1(b). Figure 2 shows the

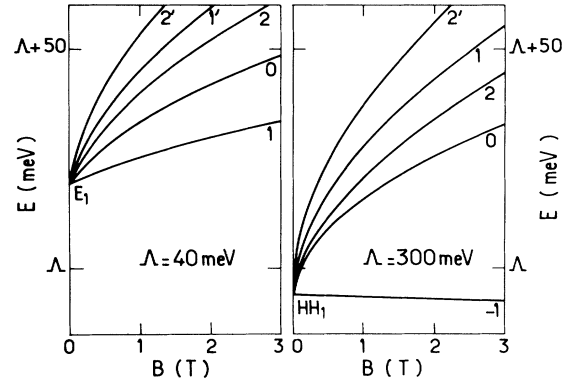


FIG. 2. Calculated conduction Landau-level energies in S_1 in the (a) semiconducting and (b) semimetallic configurations.

calculated conduction Landau levels in S_1 when a magnetic field B is applied along the growth axis.⁸ Note the very large nonlinearity of the Landau-level energies versus B which corresponds to the strong nonparabolicity of the conduction band along k_x (Fig. 1). The cyclotron resonance corresponds to the $1 \rightarrow 2$ transition for $\Lambda = 40$ meV (semiconductor) and to the $-1 \rightarrow 0$ transition for $\Lambda = 300$ meV (semimetal).

The magnetoabsorption experiments were done at 1.6 K using a molecular gas laser ($\lambda = 41$ -255 μm). The transmission signal was measured at fixed infrared photon energies E , while B could be varied up to 12 T. Figure 3 shows the transmission spectra in S_1 and S_2 at $\lambda = 118 \mu\text{m}$ for $\theta = 0$ (Faraday geometry), 45° , and 90° (Voigt geometry), where θ is the angle between the direction of B and the SL growth axis. For $\theta = 0$, two well-developed resonance lines (HWHM < 0.1 T) are observed, occurring at low B (< 1 T). When θ is increased, the transmission minima are shifted towards higher magnetic fields. Note that a $\cos\theta$ dependence is

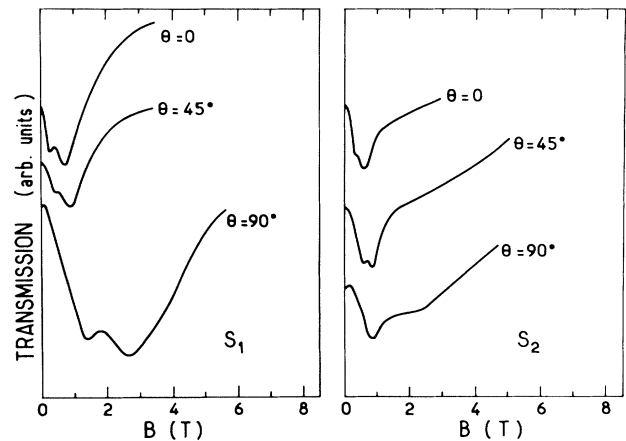


FIG. 3. Transmission spectra obtained at $\lambda = 118 \mu\text{m}$ for $T = 1.6$ K.

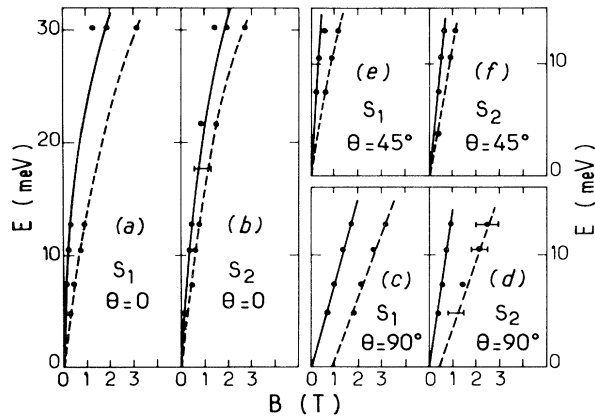


FIG. 4. Energy of the transmission minima vs B . The solid line at $\theta=0$ is the calculated SL cyclotron resonance using $\Lambda=300$ meV. The solid lines at $\theta\neq 0$ are the calculated transitions using the ellipsoidal approximation as described in the text. The dashed lines are only guides for the eye.

observed between $\theta=0^\circ$ and $\theta=45^\circ$ for the position of the resonances. The energy of the transmission minima is shown versus B in Fig. 4 for S_1 and S_2 . For $\theta=0$ [Figs. 4(a) and 4(b)], the two observed transitions extrapolate to $E\approx 0$ at $B=0$ and are thus attributed to electron cyclotron resonances taking into account the n -type nature of the samples. The solid line in Figs. 4(a) and 4(b) is the calculated SL cyclotron resonance using $\Lambda=300$ meV (i.e., the $-1\rightarrow 0$ transition in Fig. 2). For both samples, the agreement is quite satisfying and one can therefore reasonably consider that the lower-field line is due to the SL electron cyclotron resonance. The cyclotron masses determined at low B (< 0.2 T) are $m_c = 2.5 \times 10^{-3} m_0$ and $3.6 \times 10^{-3} m_0$ for S_1 and S_2 , respectively, in good agreement with m_x values determined from the dispersion relation near $k_x=0$. Such masses are considerably smaller than the electron mass in bulk $\text{Hg}_{0.95}\text{Zn}_{0.05}\text{Te}$ which is $\approx 1.5 \times 10^{-2} m_0$. Indeed, in a type-III SL, the in-plane electron and hole masses result from the $\mathbf{k}\cdot\mathbf{p}$ interaction between HH_1 and E_1 along k_x , and the situation is quite similar to that encountered in bulk $\text{Hg}_x\text{Cd}_{1-x}\text{Te}$ near the semimetal \rightarrow semiconductor transition.^{1,3} The HH_1 - E_1 separation energy is calculated to be a few meV's in S_1 and S_2 for $\Lambda=300$ meV. Besides, one has to consider that, in heterostructures grown in the [100] direction, a charge transfer could occur between the CdTe buffer layer and the SL, as reported in (100) HgCdTe -CdTe heterostructures.¹⁵ The higher-field resonance could thus be interpreted as the electron cyclotron resonance of the 2DEG formed in the SL at the interface with the CdTe buffer layer. The electron 2DEG density, obtained from magnetotransport measurements, is a few 10^{11} cm^{-2} as reported previously¹⁵ in (100) II-VI heterostructures. For this density range, it is well known that the 2DEG spatial extension

along z is very large in a small-gap material with light electron effective mass; for instance, in HgCdTe alloys, it can be as large as $\approx 1000 \text{ \AA}$.¹⁶ In S_1 and S_2 , the small-gap material is the SL and the 2DEG extension along z is expected to be much larger than the SL period, even if an exact calculation would be very intricate in that case. The 2DEG is therefore confined within the SL and not simply in a single quantum well as in usual modulation-doped III-V heterostructures. The observation of a larger cyclotron mass in the 2DEG, as compared to the SL mass, is simply due to nonparabolicity effects. Calculations done with $\Lambda=40$ meV could also fit correctly the data at $\theta=0$, even if the agreement between theory and experiment is better with $\Lambda=300$ meV.

In the Voigt geometry ($\theta=90^\circ$), the low-field transition shown in Figs. 4(c) and 4(d) corresponds to the SL cyclotron resonance and occurs at magnetic fields for which the cyclotron orbit radius is larger or comparable to the SL period. The electrons are then forced to execute cyclotron motion by tunneling through the interfaces. We have not calculated the Landau-level energies for $\theta\neq 0$ and, to interpret the position of the low-field line as a function of θ , we simply assume that the conduction band is ellipsoidal around $k=0$. At low B , the cyclotron mass is given by¹⁷ $m_c^2 = m_x^2 m_z / (m_z \cos^2 \theta + m_x \sin^2 \theta)$, yielding $m_c = (m_x m_z)^{1/2}$ for $\theta=90^\circ$. From Figs. 4(c) and 4(d), we deduce $m_z = 0.10 m_0$ in S_1 and $m_z = 0.019 m_0$ in S_2 . The experimental mass-anisotropy ratio m_z/m_x at low B (< 0.2 T) is ≈ 40 for S_1 and ≈ 5 for S_2 , and it decreases with the CdTe layer thickness, as expected from the band-structure calculations. These measurements clearly support the semimetallic character of S_1 and S_2 . Indeed, calculations using $\Lambda=40$ meV (in the semiconducting configuration) should give an anisotropy ratio less than 2 for S_1 [see Fig. 1(a)] and < 1 for S_2 , far from the experimental values. The heavier m_z measured at low B shows that the conduction band is in fact nearly flat along k_z near $k_z=0$, in agreement with the semimetallic band structure calculated for $\Lambda=300$ meV which is shown in Fig. 1(b) for S_1 . It is important to point out that the experimental values of m_z correspond neither exactly to the HH_1 dispersion relation along k_z nor to that of E_1 , but to an intermediate dispersion. We believe that this is a consequence of the HH_1 - E_1 anticrossing along k_z . For photon energy larger than 15 meV, the results in the Voigt configuration become quite intricate and a detailed analysis of the data would require calculations of the Landau levels for $\theta=90^\circ$. Furthermore, it is well known that cyclotron resonance in the Voigt geometry does not occur at $\omega_c = eB/m_c$ but at a frequency $\omega = (\omega_c^2 + \omega_p^2)^{1/2}$, where ω_p is the plasma frequency. As shown by the lower-field transition in Figs. 4(c) and 4(d), we have not observed any plasma shift of the SL cyclotron resonance, so that $\hbar\omega_p < 5$ meV since this is the lowest photon energy in

the measurements. Even if the exact expression of ω_p a type-III SL is unknown, we believe that this is consistent¹⁸ with the low carrier density ($\approx 10^{15} \text{ cm}^{-3}$) measured in S_1 and S_2 at 1.6 K. As a consequence of the strong conduction-band anisotropy ($m_z \gg m_x$), the cyclotron mass m_c for $0 \leq \theta \leq 45^\circ$, where $\sin\theta < \cos\theta$, is given in the ellipsoidal approximation by $m_c \approx m_x/\cos\theta$. This explains the cosine dependence observed for $\theta = 45^\circ$ [solid lines in Figs. 4(e) and 4(f)], which could not be interpreted in the semiconducting configuration.

The higher-field transition in Figs. 4(c) and 4(d) does not extrapolate to $B=0$ for $E=0$. Such a behavior was also reported in p -type HgTe-CdTe SL⁵ and tentatively identified as a spin-resonance line. Another possible explanation is once again the existence of a 2DEG in the SL at the interface with the buffer layer in the (100) structures. For B parallel to the plane of a 2DEG with several populated electric subbands, mixed electric and magnetic levels are formed and transitions between hybrid levels can be observed as in InAs-GaSb heterojunctions.¹⁹ Such transitions are found to extrapolate to a finite value of B for $E=0$.

In conclusion, we have measured the conduction-band dispersion in a novel type-III SL system, HgZnTe-CdTe, from cyclotron-resonance techniques. The samples were n type with a high electron mobility, while most of the results reported previously on type-III SL's were obtained on p -type materials. We have demonstrated that the mass-anisotropy ratio increases very rapidly with the CdTe layer thickness, which is an important result for the applications of type-III SL's as new infrared materials.²⁰ The rather large anisotropy ratio measured at low magnetic field shows clearly that the samples are semimetallic and can only be interpreted theoretically by using a large valence-band offset $\Lambda \approx 300 \text{ meV}$ between $\text{Hg}_{0.95}\text{Zn}_{0.05}\text{Te}$ and $\text{Hg}_{0.15}\text{Cd}_{0.85}\text{Te}$, which corresponds to $\Lambda \approx 350 \text{ meV}$ between HgTe and CdTe, in agreement with XPS measurements.¹¹ Calculations using $\Lambda = 40 \text{ meV}$ can account for the in-plane cyclotron resonance but not for the data obtained in tilted magnetic field. We have also checked in a similar SL corresponding to a semiconductor situation that the measured masses (m_x, m_z) are in good agreement with the calculated E_1 band dispersion for $\Lambda = 300 \text{ meV}$. Finally, the existence of a 2DEG at the interface between the CdTe buffer layer and the (100) SL is strongly evidenced and charge-transfer effects must be considered in (100) mercury-

based heterostructures.

Two of the authors (X.C. and J.P.F.) would like to acknowledge partial support of this work by SDIO/IST/NRL under Contract No. N00014-86-K-2023.

¹N. F. Johnson, P. M. Hui, and H. Ehrenreich, *Phys. Rev. Lett.* **61**, 1993 (1988).

²J. P. Faurie, M. Boukerche, S. Sivananthan, J. Reno, and C. Hsu, *Superlattices Microstruct.* **1**, 237 (1985).

³J. R. Meyer, C. A. Hoffman, F. J. Bartoli, J. W. Han, J. W. Cook, J. F. Schetzina, X. Chu, J. P. Faurie, and J. N. Schulman, *Phys. Rev. B* **38**, 2204 (1988).

⁴T. Duffield, R. Bhat, M. Koza, F. De Rosa, D. M. Hwang, P. Grabbe, and S. J. Allen, *Phys. Rev. Lett.* **56**, 2724 (1986).

⁵J. M. Perez, R. J. Wagner, J. R. Meyer, J. W. Han, J. W. Cook, and J. F. Schetzina, *Phys. Rev. Lett.* **61**, 2261 (1988).

⁶X. Chu, S. Sivananthan, and J. P. Faurie, *Superlattices Microstruct.* **4**, 175 (1988); *SPIE* **878**, 42 (1988).

⁷J. Reno, R. Sporken, Y. J. Kim, C. Hsu, and J. P. Faurie, *Appl. Phys. Lett.* **51**, 1545 (1987).

⁸J. M. Berroir, Y. Guldner, J. P. Vieren, M. Voos, and J. P. Faurie, *Phys. Rev. B* **34**, 891 (1986).

⁹A. Sher, D. Eger, A. Zemel, H. Feldstein, and A. Raizman, *J. Vac. Sci. Technol. A* **4**, 2024 (1986).

¹⁰Y. Guldner, G. Bastard, J. P. Vieren, M. Voos, J. P. Faurie, and A. Million, *Phys. Rev. Lett.* **51**, 907 (1983).

¹¹S. P. Kowalczyk, J. T. Cheung, E. A. Kraut, and R. W. Grant, *Phys. Rev. Lett.* **56**, 1605 (1986); Tran Minh Duc, C. Hsu, and J. P. Faurie, *ibid.* **58**, 1127 (1987).

¹²F. H. Pollak and M. Cardona, *Phys. Rev.* **172**, 816 (1968).

¹³G. Y. Wu and T. C. McGill, *Appl. Phys. Lett.* **47**, 634 (1985).

¹⁴J. M. Berroir and J. A. Brum, *Superlattices Microstruct.* **3**, 239 (1987).

¹⁵Y. Guldner, G. S. Boebinger, J. P. Vieren, and M. Voos, *Phys. Rev. B* **36**, 2958 (1987).

¹⁶Y. Takada, K. Arai, and Y. Uemura, in *Physics of Narrow Gap Semiconductors*, edited by E. Gornik, H. Heinrich, and L. Palmetzhofer, *Lecture Notes in Physics* Vol. 152 (Springer, Heidelberg, 1982), p. 101.

¹⁷N. W. Ashcroft and N. D. Mermin, *Solid State Physics* (Holt, Rinehart and Winston, New York, 1976), p. 571.

¹⁸Using the well-known bulk expression for ω_p , $n = 10^{15} \text{ cm}^{-3}$ at 1.6 K, and an average m_x, m_z mass of $10^{-2}m_0$, we get $\hbar\omega_p \sim 3 \text{ meV}$.

¹⁹J. C. Maan, C. Uihlein, L. L. Chang, and L. Esaki, *Solid State Commun.* **44**, 653 (1982).

²⁰D. L. Smith, T. C. McGill, and J. N. Schulman, *Appl. Phys. Lett.* **43**, 180 (1983).